RSC Advances

PAPER

View Article Online
View Journal | View Issue

Cite this: *RSC Adv.*, 2026, **16**, 1344

Study on the synthesis and biological activity of kojic acid–piperazine derivatives

Meiqun Ye, Xiqian Xie, Yinxing Chen, Hui Jiang, Man Ren and Jinbing Liu*

Tyrosinase inhibitors have potential applications in pharmaceutical and cosmetic products, and also in the food industry. This study aimed to discover novel tyrosinase inhibitors with high inhibitory activity and low toxicity. A series of kojic acid–piperazine derivatives were designed and synthesized, and their biological activities, including anti-tyrosinase, antioxidant, and anti-browning effects, were investigated. Several compounds exhibited significant tyrosinase inhibitory activity. Among them, compound **3o** showed the strongest activity, with an IC_{50} value of 0.21 μM, which was significantly lower than that of the positive control, kojic acid. The mechanism of tyrosinase inhibition was further investigated using compound **3o**. Kinetic studies indicated that it acts as a competitive inhibitor (K_i = 0.209 μM, K_{is} = 0.93 μM). Fluorescence quenching experiments confirmed a dynamic quenching mode. Furthermore, molecular docking and FT-IR studies revealed that compound **3o** binds to the C=O and N–H bonds of tyrosinase. Specifically, its kojic acid fragment interacts with the copper ion active site and adjacent amino acid residues, while the piperazine ring fragment forms π–π interactions with other residues. Additionally, compound **3o** demonstrated notable anti-browning and antioxidant activities, exhibited low cytotoxicity. In conclusion, these findings highlight compound **3o** as a highly promising candidate, providing a valuable molecular framework for developing novel, efficient, and safe tyrosinase inhibitors with potent antioxidant and anti-browning capabilities.

Received 30th October 2025
Accepted 21st December 2025

DOI: 10.1039/d5ra08323k

rsc.li/rsc-advances

1. Introduction

Tyrosinase (tyrosinase precursor, GenBank: EC 1.14.18.1) serves as a key rate-limiting enzyme in melanin synthesis and is also a major factor in enzymatic browning in fruits and vegetables.[1–4] In the melanogenesis process, tyrosinase catalyzes the oxidation of *L*-tyrosine to *L*-3,4-dihydroxyphenylalanine (*L*-DOPA) and further oxidizes *L*-DOPA into o-quinone, ultimately leading to melanin production. Melanin is a high-molecular-weight biological pigment primarily distributed in mammalian epidermal and keratinocyte cells, determining skin and hair color while protecting the skin from UV-induced DNA damage.[5,6] However, abnormal melanin deposition can lead to hyperpigmentation issues such as age spots and freckles, and may even trigger malignant transformation, resulting in melanoma.[7–9] Disorders in melanogenesis seem to be linked to neurodegenerative pathologies, including Parkinson's, Alzheimer's, and Huntington's diseases.[10] Additionally, tyrosinase plays roles in insect molting and wound healing.[11] Therefore, developing highly effective and low-toxicity tyrosinase inhibitors holds significant importance for advancing the food industry, medicine, and agriculture.

Oxidative stress, an imbalance between antioxidant systems and the production of oxidants, mainly induced by reactive oxygen species (ROS), leads to oxidative degradation of biomolecules.[12,13] An appropriate amount of ROS can participate in regulating cell signaling pathways, inducing and promoting mitotic reaction, maintaining redox homeostasis and fighting infection factors.[14] Excessive ROS can damage DNA, protein, nucleic acid and lipid, and can also cause excessive oxidative reaction, leading to human aging and a variety of chronic diseases, such as cancer, cardiovascular disease, hypertension, atherosclerosis, diabetes, neurodegenerative disease.[15] The overall anti-oxidant potential of a specific compound depends upon the variable contribution of features as the free radical scavenging capacity, the reducing and redox buffering effectiveness, and the metal-chelating properties. In addition, free radicals also play an important role in the biosynthesis of melanin, and some studies have shown that free radicals are involved in the catalytic reactions of tyrosinase. Several active compounds with antioxidant activity and tyrosinase activity have been reported.[16] Thus the antioxidant effect in cosmetics such as whitening agents is highly considered.

Researchers have conducted extensive studies to develop novel tyrosinase inhibitors and antioxidants. Numerous chemically synthesized and naturally derived candidates have been reported. Currently marketed tyrosinase inhibitors, such as kojic acid derivatives, hydroquinones, and arbutin, exhibit

School of Food and Chemical Engineering, Shaoyang University, Shao Shui Xi Road, Shaoyang 422100, People's Republic of China. E-mail: syuliujb@163.com

some limitations including high cost, significant side effects, moderate efficacy, and poor stability.[17,18] Kojic acid and its derivatives demonstrate a wide range of pharmacological profiles, such as antityrosinase, antioxidant, antibacterial, antitumor, anti-inflammatory, antiproliferative activities.[19,20] Kojic acid has been used in food preservation, anti-browning, and skin whitening.[21] However, the use of kojic acid in cosmetics is currently limited due to its cytotoxicity, chemical instability, and low lipophilicity, which may result in skin irritations.[22] Besides, several adverse effects including genotoxic, hepatocarcinogenic, and allergic dermatitis have also been involved during its clinical use.[23] Subsequently, another well-known tyrosinase inhibitor, hydroquinone, can lead to erythema, stinging, colloid milium, allergic contact dermatitis, nail discoloration, and paradoxical postinflammatory hypermelanosis.[24] Based on these severe side effects, recent EU (European Union) cosmetic regulations have restricted or even banned the use of kojic acid and hydroquinone as skin whitening agents.[25] To overcome the above-mentioned shortcomings of kojic acid, the hydroxypyranone structure of kojic acid as a good pharmacophoric unit for the design of new tyrosinase inhibitors.[26,27] In fact, several kojic acid derivatives have also been developed as the new generation of anti-browning and antioxdant agents.[28–32] Piperazine, a privileged nitrogen-containing heterocycle, displays anticancer, antimicrobial, antiviral activities.[33,34] Also, piperazine is located in the structures of some vital drugs such as ciprofoxacin, levofoxacin, aplaviroc and imatinib.[35,36] Notably, acylpiperazine derivatives exhibit promising tyrosinase inhibition.[37,38] H-bond interactions between the piperazine nitrogen atom and the crucial residues could be found; moreover, π–π stacking interactions between the carbonyl group of the amide moiety and the crucial residues could be established.[39] A recent study of Karakaya reported that kojic acid–benzylpiperazine hybrids exhibits potent tyrosinase inhibitory activity.[33] Given these advantages, and inspired by the principle of active skeleton hybridization in compound design, we reasoned that the proper hybridization of kojic acid and piperazine motif might be feasible for developing a new tyrosinase inhibitors and antioxidants with high activity and low toxicity.

As part of ongoing efforts to discover potent tyrosinase inhibitors with minimum side effects, in the present study, kojic acid–piperazine hybrids were designed and synthesized. Subsequently, their structure–activity relationships regarding the inhibition of mushroom tyrosinase were primarily discussed. Besides, the inhibition mechanism, the mode of action, the antioxidant activity, the anti-browning effect were also systematically investigated. This study establishes a foundation for optimizing kojic acid–derived tyrosinase inhibitors with improved inhibitory activity and low toxicity.

2. Results and discussion

2.1. Chemistry

The synthesis route of kojic acid–benzylpiperazine hybrids is shown in Scheme 1. Briefly, *N*-Boc-benzoylpiperazine

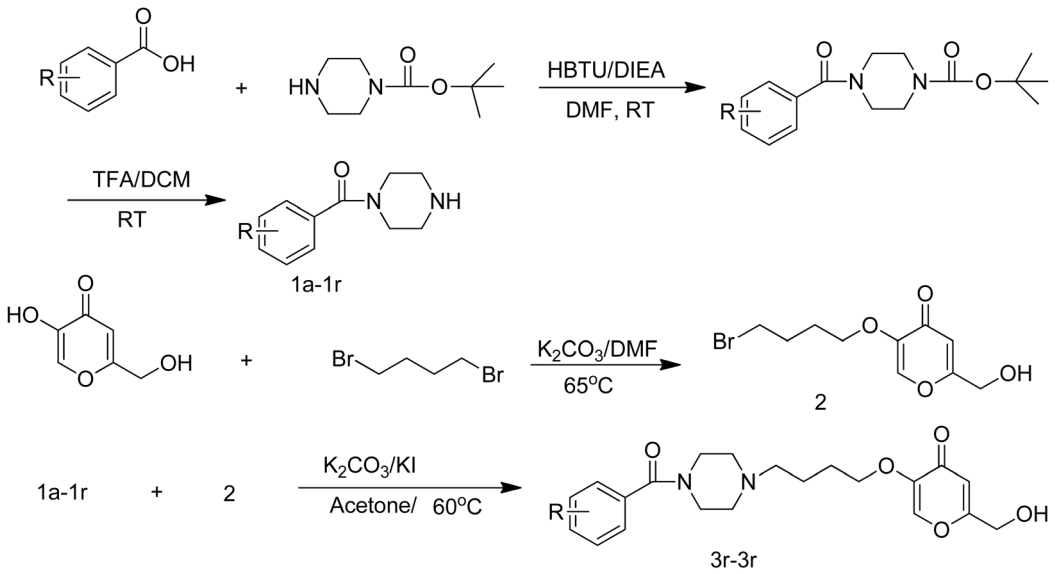

3a R = H; 3b R = 3-CH_3; 3c R = 4-CH_3; 3d R = 2-OCH_3; 3e R = 3-OCH_3;
3f R = 4-OCH_3; 3g R = 2-F; 3h R = 3-F; 3i R = 4-F; 3j R = 2-Cl;
3k R = 3-Cl; 3l R = 4-Cl; 3m R = 2-Br; 3n R = 3-Br; 3o R = 4-Br;
3p R = 2-CF_3; 3q R = 3-CF_3; 3r R = 4-CF_3

Scheme 1 Synthesis pathway of kojic acid–piperazine hybrids.

derivatives were synthesized by the reaction of Benzoic acid or substituted benzoic acids with *N*-Boc-piperazine in *N*,*N*-dimethylformamide (DMF) at room temperature for 24 hours in the presence of o-benzotriazole-*N*,*N*,*N*′,*N*′-tetramethyluronium hexafluorophosphate (HBTU) and *N*,*N*-diisopropylethylamine (DIEA). Then, *N*-Boc-benzoylpiperazine derivatives reacted with trifluoroacetic acid (TFA) to give benzoylpiperazine derivatives. Etherification of 1,4-dibromobutane and kojic acid was carried out in DMF at 65 °C in the presence of K_2CO_3. Compounds **3a–3r** were prepared by stirring the mixture of the corresponding benzoylpiperazine derivative and ether intermediate in acetone at 65 °C in the presence of K_2CO_3 and KI. The synthesized compounds were characterized by ^{1}H-NMR, ^{13}C-NMR, IR and HR-MS.

2.2. Tyrosinase inhibitory activity

The tyrosinase inhibition measurements of compounds **3a–3r** were carried out using *L*-DOPA as substrate, each concentration was analyzed in three independent experiments run in triplicate. Kojic acid was selected as a positive control compound. The inhibitory activities of the kojic acid–benzylpiperazine hybrids against tyrosinase were presented in the Table 1. From the Table 1, except for compound **3b** (R = 3-CH_3), compound **3e** (R = 3-OCH_3), compound **3h** (R = 3-F), compound **3k** (R = 3-Cl) and compound **3n** (R = 3-Br), the other compounds showed better inhibitory effects on tyrosinase than the positive control inhibitor kojic acid, and compound **3o** was the most potent tyrosinase inhibitor with IC_{50} value of 0.21 ± 0.01 μM. The reason of compound **3o** demonstrated stronger tyrosinase inhibitory activity than the other compounds and the positive control inhibitor kojic acid may be attributed to the following factors: The higher hydrophobicity of compound **3o** facilitates better interaction with the active site of tyrosinase; introduction of two nitrogen atoms increases the likelihood of interactions with amino acid residues in tyrosinase; larger atomic radius of bromine (compared to chlorine and fluorine) results in weaker nuclear attraction to its outer electrons, promoting stronger interactions with tyrosinase's amino acid residues. From Table 1, it can be seen that the type and position of substituents on the benzene ring have a significant impact on inhibitory activity. The structure–activity relationships (SARs) of these compounds were rationally discussed and are summarized as follows:

(1) A comparison of compound **3a**with other compounds in terms of tyrosinase inhibitory activity revealed that the presence of substituents on the benzene ring did not significantly improve inhibition. On the contrary, some *meta*-substituted compounds, such as **3b** (R = 3-CH_3), **3e** (R = 3-OCH_3), **3k** (R = 3-Cl), and **3n** (R = 3-Br), completely lost their inhibitory activity, which may be attributed to increased steric hindrance.

(2) When electron-donating groups are attached to the benzene ring, *ortho*-substituted compounds exhibit the highest activity (*e.g.*, compound **3d**, R = 2-OCH_3, IC_{50} = 0.35 ± 0.05 μM), while *meta*-substituted compounds show the weakest activity (*e.g.*, **3e**, R = 3-OCH_3, IC_{50} > 200 μM). In contrast, when electron-withdrawing groups are present on the benzene ring, *para*-substituted compounds such as **3l** (R = 4-Cl), **3o** (R = 4-Br), and **3r** (R = 4-CF_3) demonstrate strong tyrosinase inhibitory effects, with IC_{50} values all below 1 μM. However, compounds with *meta*-substituted electron-withdrawing groups (*e.g.*, **3h**, R = 3-F; **3k**, R = 3-Cl) exhibit the lowest inhibition (IC_{50} > 200 μM). This may be attributed to poor molecular symmetry and increased steric hindrance in *meta*-substituted derivatives, which likely hinder their interaction with tyrosinase.

(3) Comparing the tyrosinase inhibitory activity in halogen-substituted compounds, the brominated compounds demonstrated optimal tyrosinase inhibitory activity at their respective positions, while fluorinated analogues showed the weakest effects. Interestingly, smaller atomic radius (*F*) correlated with reduced inhibitory potency. This result may be related to the electronegativity of halogen atoms, where higher electronegativity correlates with weaker tyrosinase inhibitory activity.

(4) Comparing the tyrosinase inhibitory activity of the compounds with electron-donating groups, the methoxy-substituted compounds exhibited inferior inhibitory activity compared to their methyl-substituted counterparts at corresponding positions, which may be attributed to the conjugative effect between the oxygen atom and the benzene ring.

The above findings were also confirmed by molecular docking.

Table 1 Inhibitory tyrosinase activity of the target compounds and kojic acid

Compd	IC_{50}(μM) ± SD	Compd	IC_{50}(μM) ± SD
3a	0.40 ± 0.03	**3k**	>200
3b	>200	**3l**	0.96 ± 0.01
3c	22.37 ± 0.49	**3m**	1.34 ± 0.12
3d	0.35 ± 0.05	**3n**	92.50 ± 2.06
3e	>200	**3o**	0.21 ± 0.01
3f	102.3 ± 1.67	**3p**	2.01 ± 0.28
3g	26.73 ± 0.96	**3q**	24.62 ± 1.08
3h	>200	**3r**	0.93 ± 0.05
3i	1.59 ± 0.15	Kojic acid	34.13 ± 0.03
3j	8.33 ± 0.67		

2.3. Inhibition mechanism

Considering that compound **3o** exhibited the highest tyrosinase inhibitory activity among the tested kojic acid–benzylpiperazine hybrids, we proceeded to further explore its inhibition mechanism. Subsequently, the inhibitory type of compound **3o** on mushroom tyrosinase was identified through the Lineweaver–Burk double reciprocal plots, following treatment with varying concentrations of compound **3o** and the substrate. As illustrated in Fig. 1A, the plots of 1/*V* against 1/[S] yielded a family of straight lines with diverse slopes. Notably, the slope of the curve exhibited a downward trend as the inhibitor concentration decreased, and all of the straight lines intersected at a single point within the first quadrant. This pattern strongly suggested that compound **3o** functions as a competitive inhibitor. To determine the inhibition constant (K_i) of the compound, a plot was constructed with the slope values plotted against the

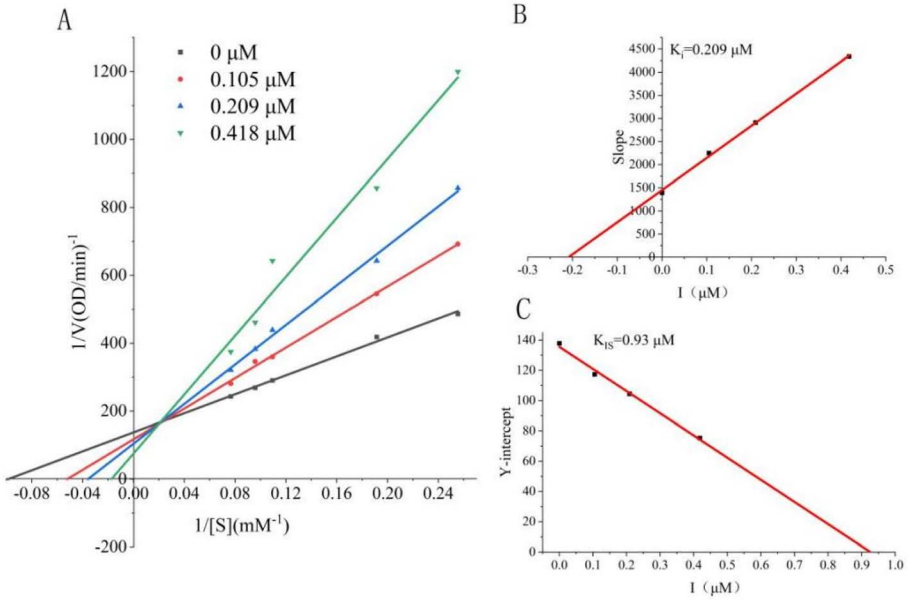

Fig. 1 Kinetic inhibition measurement of compound **3o**. The inhibition type of **3o** was demonstrated through the Lineweavere–Burk plot. (A) In this figure, the concentrations of **3o** were 0 μM, 2 μM, and 4 μM, respectively. (B) The secondary replot was constructed by plotting the slope against the concentrations of **3o**, which was used to determine the inhibition constant K_i. (C) The secondary replot in this case involved plotting the intercept against the concentrations of **3o**, aiming to define the inhibition constant K_{is}.

concentrations of compound **3o**. Additionally, a plot of the vertical intercept $(1/V_m)$ against the concentrations of compound **3o** was generated to obtain the K_{is} value of the compound. As depicted in Fig. 1B and C, the K_i value and the K_{is} value of the compound were calculated to be 0.209 μM and 0.93 μM, respectively. $K_{is} > K_i$, compound **3o** demonstrates superior binding affinity to the free enzyme.

2.4. Fluorescence quenching

Fluorescence quenching means that some small molecule compounds bind to protein that can affect the fluorescence intensity of the fluorophore. Therefore, in order to obtain information about conformational changes of enzymes, fluorescence spectroscopy has become a very important research tool. Fluorescence spectra of tyrosinase with different concentrations of compound **3o** were investigated, as shown in Fig. 2. With increasing concentrations of compound **3o**, the dramatically decreasing fluorescence intensity of tyrosinase could be found. This suggested the inhibitor had potent quenching effect on the fluorescence of tyrosinase. At the same time, there was no significant red shift or blue shift in the fluorescence emission peak of tyrosinase after the addition of compound **3o**. This result showed that the interaction between the sample and tyrosinase did not change the hydrophobic environment in the vicinity of the chromophore tryptophan residues. Moreover, it was also indicated that the predominant quenching mechanism of compound **3o** was likely to be dynamic quenching, as the quenching constant increased with a rise in temperature. The quenching of the intrinsic fluorescence furnished direct and unequivocal evidence that the inhibitor compound **3o** was capable of binding to tyrosinase. The binding of compound **3o** to tyrosinase induced a change in the microenvironment surrounding the fluorophore. The detailed values of K_{sv} and K_q are summarized in Table 2.

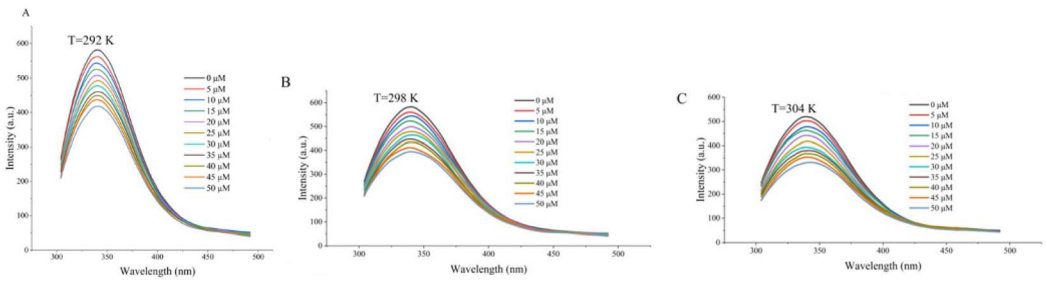

Fig. 2 Fluorescence emission spectra of tyrosinase with different concentrations of compound **3o** (λ_{ex} = 280 nm, (A): T = 292 K, (B): T = 298 K, (C): T = 304 K). The final enzyme concentration was 0.05 mg mL^{-1}, and c (compound **3o**) = 0 μM, 5 μM, 10 μM, 15 μM, 20 μM, 25 μM, 30 μM, 35 μM, 40 μM, 45 μM, 50 μM for the curves from top to bottom, respectively.

Table 2 Stern–Volmer equation parameters (quenching constants K_{SV}, biomolecular quenching rate constant Kq) for the interaction between compound **3o** and tyrosinase

T/K	R^2	K_{SV} (L^{-1} μmol^{-1})	Kq (L^{-1} μmol^{-1} s^{-1})
292	0.99218	0.00743	7.43×10^7
298	0.98678	0.00952	9.52×10^7
304	0.99656	0.01123	11.23×10^7

2.5. FT-IR spectrum

FT-IR spectroscopy has been widely used to study the secondary structure conformation of small molecules and proteins systems. Amide I band (1600–1800 cm^{-1}) is ascribed to the stretching vibration of C=O group, and amide II band (3300–3500 cm^{-1}) corresponds to the bending vibration of N–H.[40] The interaction between compound **3o** and tyrosinase was studied by FT-IR spectroscopy (Fig. 3). The spectral results indicated that the characteristic peak of the amide I band shifted from 1639.97 cm^{-1} to 1636.47 cm^{-1} and the characteristic peak of the amide II band shifted from 3415.29 cm^{-1} to 3446.43 cm^{-1}. The results showed that the compound **3o** interacted with the C=O and N–H moieties of polypeptides and caused a rearrangement in the folding conformation, resulting in potential inhibitory activity against tyrosinase.

2.6. Molecular docking study

To clarify whether compound **3o** binds directly to tyrosinase, we conducted a molecular docking study using Discovery Studio 2019 software (Fig. 4A and B). As demonstrated in Fig. 4A. Compound **3o** was identified as a competitive inhibitor *via* kinetic assay. In Fig. 4, the results revealed that the kojic acid fragment within compound **3o** penetrated the bottom of the tyrosinase activity site pocket. Notably, it not only overlapped precisely with the original ligand in the crystal structure but also showed a remarkable overlap with kojic acid itself. The carbonyl group of the kojic acid fragment and oxygen atom of ether bond interacted with copper ions, maintaining the bond lengths of 2.9 Å and 3.4 Å, respectively. These results demonstrate that compound **3o** competes with the substrate for binding to the enzyme's active site, confirming its classification as a competitive inhibitor, which is consistent with the kinetic assay data of tyrosinase inhibition. Meanwhile, the 5-hydroxyl substituent on the pyranone ring formed hydrogen bond with Glu256 and His 244, with the bond lengths of 2.5 Å and 2.0 Å, respectively. This result also serves as a key mechanistic explanation for the compound **3o** with superior tyrosinase inhibitory activity. Additionally, the piperazine fragment exhibits notable π–π interactions with Phe264, a key amino acid at the base of tyrosinase active site (Fig. 4B, red dashed line), which further contributes to superior tyrosinase inhibitory activity of the compound **3o**. The results demonstrate that incorporating the kojic acid scaffold and piperazine ring into a single molecule is advantageous for enhancing inhibitory activity.

The kojic acid fragment of compound **3o** penetrates into the bottom of the active pocket of human tyrosinase (PDB ID:5 M8M) (Fig. 4C). Carbonyl group of Kojic acid forms a strong metal–ligand interaction with the active center of human tyrosinase, with a bond length of 2.4 Å (Fig. 4D). Hydroxy group of Kojic acid forms hydrogen bond with Thr-391 (2.4 Å). The amide group fragment forms hydrogen bond with Arg-374 (2.9 Å).

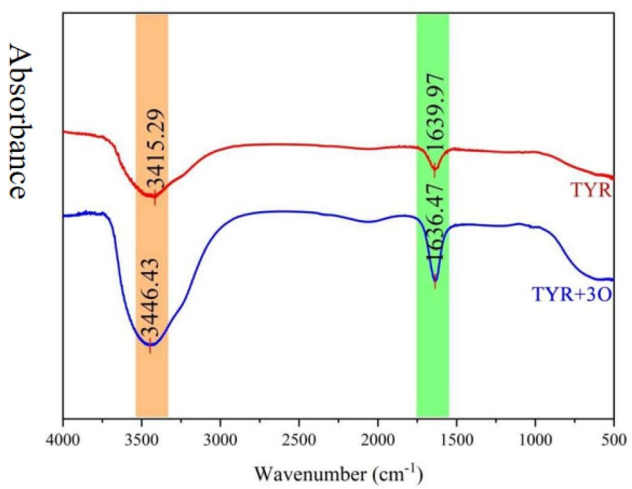

Fig. 3 FT-IR spectra of tyrosinase and tyrosinase + compound **3o**.

2.7. Anti-browning study

Among the synthesized target compounds, the candidate compound **3o** showed the best tyrosinase inhibitory activity. Therefore, we further evaluated its anti-browning effect on apple, in which kojic acid and Vitamin C were used as positive control. The color value change of post-cut apple treated with compound **3o** (25 μM, 50 μM, 100 μM), blank control group, kojic acid (50 μM) and Vitamin C (50 μM) during storage at 5 °C was recorded. The L^* values of the compound **3o** (25 μM) group, compound **3o** (50 μM) group, compound **3o** (100 μM) group, kojic acid group, Vitamin C group and blank group were gradually decreased, after storage at 5 °C for 5 days. The L^* values of the different concentration compound **3o** groups were not only significantly larger than blank control group but also slight larger than both Vitamin C and kojic acid (Fig. 5A). During the measurement (0–5 days), the browning extent of the apple slices in the treatment groups was obviously lower than the browning extent of the apple slices in the blank control group, kojic acid group and Vitamin C group (Fig. 5B). Furthermore, the color of the apple slices in the compound **3o** group is lighter than the color of the positive group after storage at 5 °C for 5 days. The results further suggested that compound **3o** could be used as a potent anti-browning agent, and the anti-browning ability became stronger with the increase of concentration.

2.8. Antioxidant activities

From Table 3, it can be observed that some compounds exhibited moderate DPPH radical scavenging activity. Six compounds showed better DPPH radical scavenging activity than the positive control V_C, and the compound **3h** demonstrated the strongest scavenging capacity. However, most compounds showed no ABTS radical scavenging activity.

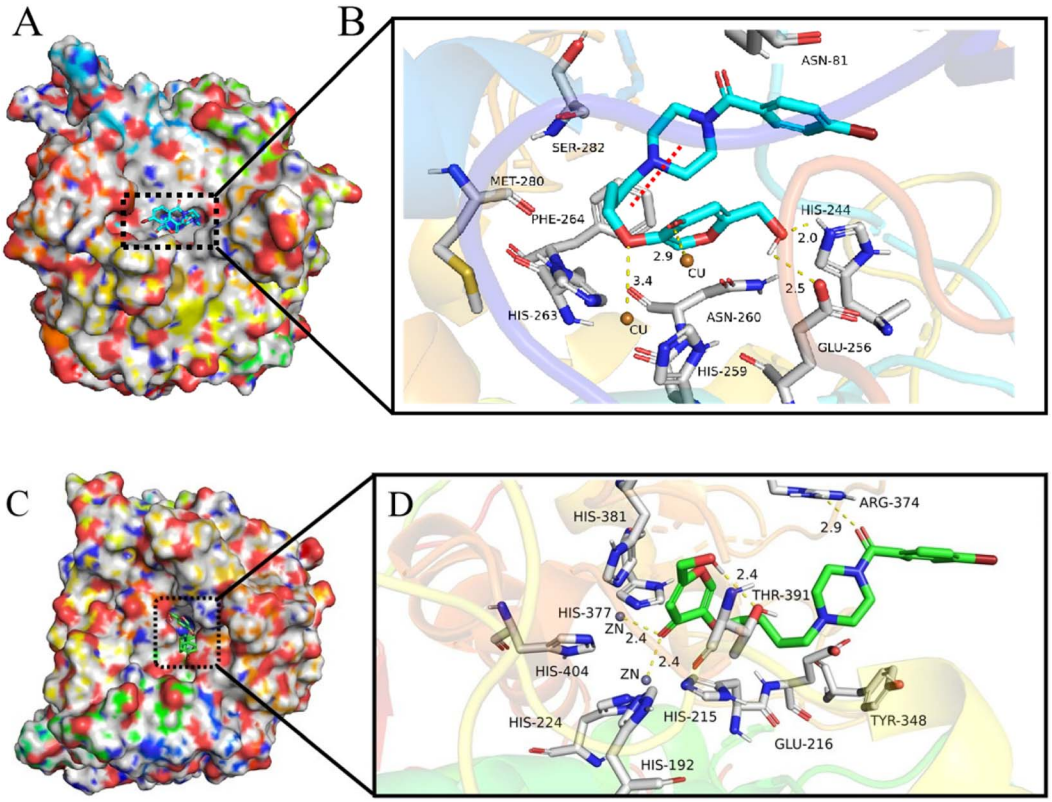

Fig. 4 (A) Docking model showing the best binding pose of compound **3o** to tyrosinase. (B) The schematic representation of the interactions of compound **3o** within the binding pocket of mushroom tyrosinase, which is derived from the docking model. Dashed lines indicate the bond distances between the interacting functionalities of the ligand and the receptor. The legends inset display the type of interaction between the ligand atoms and the amino acid residues of the protein. The pose of **3o** (cyan) and Kojic acid (yelow) in Human Tyrosinase LBD (C); The proposed interaction network between **3o** and Human Tyrosinase LBD (PDB ID:5 M8M) (D).

Compound **3a** (R = H) and compound **3l** (R = 4-Cl) displayed measurable activity against both DPPH and ABTS radicals. *Fluoro*-substituted analogues except for compound **3h** showed negligible antioxidant effects. *Chloro*-substituted derivatives (compound **3j**, compound **3k** and compound **3k**) exhibited moderate DPPH radical scavenging activity and showed superior DPPH scavenging activity compared to V_C. However, only *para-chloro* substituted compound demonstrated some ABTS scavenging activity. *Para-bromo* substituted compound (compound **3o**) exhibited certain DPPH scavenging activity,

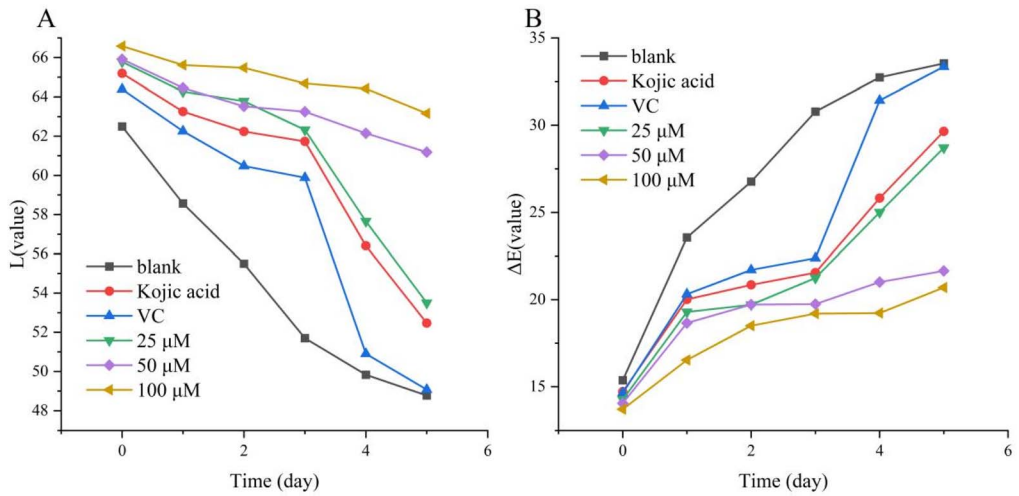

Fig. 5 (A) L* of fresh-cut apple treated with 50 μM kojic acid, 50 μM V_C or different compound **3o** solutions during the 5 day-storage at 5 °C. (B) Change in total color difference (Δ*E*) of treated with 50 μM kojic acid, 50 μM V_C or different compound **3o** solutions during the 5 day-storage at 5 °C.

Table 3 Antioxidant activity of the target compounds and Vitamin C

Compd	DPPH/IC_{50}(μM)	$ABTS^+$/IC_{50}(μM)	Compd	DPPH/IC_{50}(μM)	$ABTS^+$/IC_{50}(μM)
3a	47.56 ± 0.49	49.66 ± 0.72	**3k**	17.75 ± 0.65	>200
3b	26.99 ± 0.23	>200	**3l**	19.47 ± 0.33	67.88 ± 0.94
3c	>200	>200	**3m**	>200	>200
3d	154.9 ± 2.13	>200	**3n**	>200	>200
3e	>200	>200	**3o**	58.09 ± 0.86	>200
3f	86.41 ± 0.68	130.00 ± 2.09	**3p**	194.9 ± 3.08	>200
3g	94.99 ± 1.03	>200	**3q**	>200	160.70 ± 2.90
3h	2.39 ± 0.15	>200	**3r**	55.61 ± 0.96	>200
3i	>200	>200	V_C	53.49 ± 0.55	31.45 ± 0.68
3j	50.70 ± 0.87	>200			

however, the other *bromo*-substituted compounds possess no antioxidant activity. *Para*-CF_3 substituted compound (compound **3r**) exhibited certain DPPH scavenging activity, *ortho*-CF_3 substituted compound (compound **3p**) possesses slight DPPH scavenging activity and *meta*-CF_3 substituted compound (compound **3q**) shows slight ABTS scavenging activity.

2.9. Cell viability assessments of compound 3o

Prompted by the foregoing results, we further evaluated the potential cytotoxicity of compound **3o** using the normal HUVEC cell line *via* an MTT assay. The experiment confirmed that compound **3o** exhibited no significant toxicity even at a concentration as high as 64 μM (Fig. 6). This finding indicates the excellent safety profile of compound **3o** for applications in treating tyrosinase-mediated disorders, food preservation, and cosmetics.

3. Experimental

3.1. General

All the reactions described below were monitored by thin layer chromatography (TLC), which was performed using Merck precoated 60F254 plates. Melting points were measured on WRS-1B melting point apparatus and are uncorrected. ^{1}H NMR and ^{13}C NMR spectra were recorded on a JNM-ECZ400S/L1 400 MHz or 500 MHz at 25 °C in DMSO-d_6 or Chloroform-*d* using tetramethyl silane (TMS) as an internal standard. Coupling constant (J) and chemical shift values were measured in hertz (Hz) and parts per million (ppm), respectively. The following abbreviations are used for ^{1}H NMR: s (singlet), d (doublet), dd (doublet of doublets), t (triplet) and m (multiplet). FT-IR spectra were obtained on a Nicolet-iS5 spectrophotometer (KBr disks). Mass-spectrometric (MS) data is reported in *m*/*z* using the Q Exactive Focus. UV-2600 spectrophotometer (Shimadzu Corporation, Tokyo, Japan) was used to record UV spectra. The fluorescence spectra of the selected compound was inspected on Cary Eclipse G9800A fluorescence spectrophotometer (Agilent Technologies Co). The colorimetric measurements was carried out by a CR-400 Minolta chronometer instrument (Konica Minolta, Osaka, Japan). The model of ultrasonic cleaning machine is SB-5200DT (Ningbo Xinzhi Biotechnology Co., Ltd). Purity for target compounds was measured by high-performance liquid chromatography (HPLC) with an Thermo Scientific UltiMate 3000. Tyrosinase, *L*-3,4-dihydroxyphenylalanine (*L*-DOPA), 1,1-diphenyl-2-picrylhydrazyl radical 2,2-diphenyl-1-(2,4,6-trinitrophenyl) hydrazyl (DPPH), 2, 2′-azino-bis(3-ethylbenzo- thiazoline-6-sulfonic acid) (ABTS), and kojic acid were purchased from Sigma–Aldrich Chemical Co (Shanghai, China). Other chemicals were obtained from commercial suppliers and used without further purification.

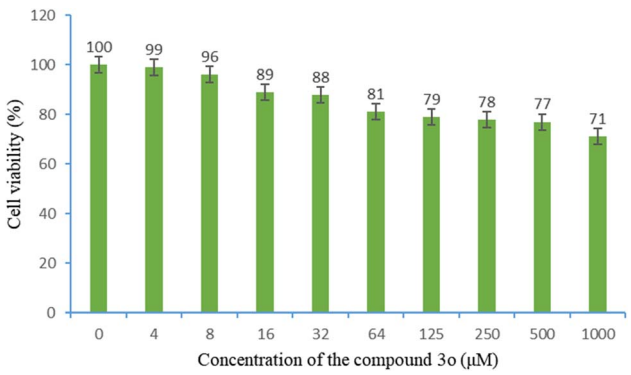

Fig. 6 The cell viability of compound **3o** in relation to human umbilical vein endothelial cells (HUVEC) is depicted.

3.2. Synthesis of 1-bromo butane kojic acid (compound 2)

Kojic acid (0.144 g, 1 mmol) and 1,4-dibromo butane (0.648 g, 3 mmol) were dissolved in 10 mL DMF, and then dried potassium carbonate 0.207 g (1.5 mmol) was added to the mixture. The reaction mixture was stirred at 65 °C for about one hour, and the reaction progress was detected by TLC (DCM : methanol = 5 : 1). After the reaction was complete, the precipitates were filtered and filtrate was extracted three times with ethyl acetate. The organic phase was combined and dried with anhydrous sodium sulfate. The solvent was removed by vacuum evaporation. The residue was purified by column chromatography to obtain 1-bromo butane kojic acid (compound **2**) with yield of 87.3%.

3.3. Synthesis of *N*-Boc-benzoylpiperazine derivatives

Benzoic acid or substituted benzoic acids (1 mmol), *N*-Boc-piperazine (0.223 g, 1.2 mmol), HBTU (0.569 g, 1.5 mmol) and DIEA (0.516 g, 4 mmol) were dissolved in 4 mL DMF. The

reaction mixture was stirred at room temperature for about 24 hours, and the reaction progress was detected by TLC (DCM : methanol = 10 : 1). After the reaction was completed and adjusted the pH to 5–6. 20 mLwater was added to the reaction mixture. The precipitates were filtered and dried to obtained *N*-Boc-benzoylpiperazine derivatives.

3.4. Synthesis of benzoylpiperazine derivatives (1a–1r)

Different *N*-Boc-benzoylpiperazine derivative (1 mmol) was dissolved in DCM(4 mL)and TFA (1 mL). The mixture reaction was stirred at room temperature for about one hour, and the reaction progress was detected by TLC (DCM : methanol = 10 : 1). After the reaction was complete and the solvent was removed by vacuum evaporation. The residue was recrystallized with diethyl ether and dried to botained the corresponding benzoylpiperazine derivative with the yield of 85–90%.

3.5. Synthesis of kojic acid–piperazine hybrids (3a–3r)

Different benzoylpiperazine derivative (1.1 mmol) and 1-bromo butane kojic acid (0.276 g, 1 mmol) were dissolved in acetone (10 mL), and then dried potassium carbonate (0.166 g, 1 mmol) and KI (0.166 g, 1 mmol) were added to the mixture. The reaction mixture was stirred at 56 °C for about 24 hours, and the reaction progress was detected by TLC (DCM : methanol = 9 : 1). After the reaction was complete, the precipitates were filtered and filtrate was concentrated by vacuum evaporation. The residue was purified by column chromatography to obtain kojic acid–piperazine hybrids.

3.5.1. 5-(4-(4-Benzoylpiperazin-1-yl)butoxy)-2-(hydroxymethyl)-4*H*-pyran-4-one (3a). Light yellow oil; Yield: 39.38%; 98.5% purity; IR (KBr, ν/cm^{-1}): 3416, 2946, 2834, 1644, 1612, 1446, 1265, 1211, 1152, 1122, 1020, 713. ^{1}H NMR (500 MHz, Chloroform-*d*) δ (ppm): 7.57 (s, 1H), 7.42–7.37 (m, 5H), 6.48 (s, 1H), 4.42 (s, 2H), 3.87 (t, J = 6.4 Hz, 2H), 3.83–3.72 (m, 2H), 3.48–3.35 (m, 2H), 2.56–2.47 (m, 2H), 2.42 (t, J = 7.4 Hz, 3H), 2.40–2.34 (m, 2H), 1.90–1.79 (m, 2H), 1.73–1.62 (m, 2H). ^{13}C NMR (125 MHz, Chloroform-*d*) δ (ppm): 174.78, 170.41, 167.47, 147.74, 139.24, 135.64, 129.77, 128.53, 127.01, 111.82, 69.41, 60.69, 57.83, 53.49, 52.77, 26.84, 23.06. HRMS (*m*/*z*) calcd. For $C_{21}H_{26}N_2O_5$ [M + H]$^+$ 387.1920, found 387.1921.

3.5.2. 2-(Hydroxymethyl)-5-(4-(4-(3-methylbenzoyl)piperazin-1-yl)butoxy)-4*H*-pyran-4-one (3b). Light yellow sticky; Yield: 28.81%; 98.2% purity; IR (KBr, ν/cm^{-1}):3305, 2923, 2818, 1650, 1613, 1454, 1295, 1210, 1149, 1030, 793, 694. ^{1}H NMR (500 MHz, DMSO-d_6) δ (ppm): 8.15 (s, 1H), 7.38 (t, J = 7.5 Hz, 1H), 7.31 (d, J = 7.6 Hz, 1H), 7.23 (s, 1H), 7.20 (d, J = 7.5 Hz, 1H), 6.35 (s, 1H), 5.83 (s, 1H), 4.35 (s, 2H), 3.87 (t, J = 6.5 Hz, 2H), 3.71–3.62 (m, 2H), 3.41–3.30 (m, 2H), 2.60–2.53 (m, 2H), 2.50–2.44 (m, 2H), 2.42–2.40 (m, 2H), 2.38 (s, 3H), 1.79–1.71 (m, 2H), 1.65–1.56 (m, 2H). ^{13}C NMR (125 MHz, DMSO-d_6) δ (ppm): 173.60, 168.44, 147.51, 140.51, 138.29, 136.40, 130.51, 127.78, 124.33, 111.36, 69.10, 59.77, 57.53, 26.82, 22.95, 21.35. HRMS (*m*/*z*) calcd. For $C_{22}H_{28}N_2O_5$ [M + H]$^+$ 401.2076, found 401.2076.

3.5.3. 2-(Hydroxymethyl)-5-(4-(4-(4-methylbenzoyl)piperazin-1-yl)butoxy)-4*H*-pyran-4-one (3c). Reddish brown sticky; Yield: 43.52%; 97.8% purity; IR (KBr, ν/cm^{-1}): 3416, 2939, 1659, 1650, 1454, 1372, 1293, 1150, 1032, 830, 753. ^{1}H NMR (400 MHz, DMSO-d_6) δ (ppm): 8.26 (s, 1H), 7.47–7.38 (m, 4H), 6.46 (s, 1H), 5.91 (s, 1H), 4.46 (s, 2H), 3.98 (t, J = 5.8 Hz, 2H), 3.81–3.65 (m, 2H), 3.60–3.42 (m, 4H), 3.37–3.30 (m, 2H), 2.67 (s, 3H), 1.91–1.80 (m, 2H), 1.76–1.65 (m, 2H). ^{13}C NMR (100 MHz, DMSO-d_6) δ (ppm): 173.55, 169.45, 168.41, 147.52, 140.55, 139.58, 133.50, 129.34, 127.49, 111.38, 69.12, 59.79, 57.54, 49.07, 26.84, 22.97, 21.37. HRMS (*m*/*z*) calcd. For $C_{22}H_{28}N_2O_5$ [M + H]$^+$ 401.2076, found 401.2073.

3.5.4. 2-(Hydroxymethyl)-5-(4-(4-(2-methoxybenzoyl)piperazin-1-yl)butoxy)-4*H*-pyran-4-one (3d). Yellow sticky; Yield: 31.72%; 98.3% purity; IR (KBr, ν/cm^{-1}): 3242, 2940, 1650, 1613, 1454, 1295, 1150, 1016, 758. ^{1}H NMR (500 MHz, DMSO-d_6) δ (ppm): 7.96 (s, 1H), 7.25 (t, J = 7.5 Hz, 1H), 7.03 (d, J = 7.0 Hz, 1H), 6.94 (d, J = 8.3 Hz, 1H), 6.86 (t, J = 7.3 Hz, 1H), 6.17 (s, 1H), 5.62 (s, 1H), 4.16 (s, 2H), 3.70–3.66 (m, 2H), 3.65 (s, 3H), 3.55–3.38 (m, 4H), 3.02–2.92 (m, 2H), 2.29–2.22 (m, 2H), 2.22–2.18 (m, 2H), 1.61–1.51 (m, 2H), 1.45–1.36 (m, 2H). ^{13}C NMR (125 MHz, DMSO-d_6) δ (ppm): 173.58, 168.42, 166.79, 155.31, 147.51, 140.49, 130.78, 128.11, 126.10, 121.09, 111.78, 111.35, 59.78, 57.58, 55.89, 53.33, 52.89, 46.74, 26.83, 22.97. HRMS (*m*/*z*) calcd. For $C_{22}H_{28}N_2O_6$ [M + H]$^+$ 417.2026, found 417.2028.

3.5.5. 2-(Hydroxymethyl)-5-(4-(4-(3-methoxybenzoyl)piperazin-1-yl)butoxy)-4*H*-pyran-4-one (3e). Yellow sticky; Yield: 43.22%; 99.2% purity; IR (KBr, ν/cm^{-1}):3271, 2940, 1650, 1612, 1454, 1294, 1149, 1032, 792, 693. ^{1}H NMR (500 MHz, DMSO-d_6) δ (ppm): 8.09 (s, 1H), 7.34 (t, J = 7.9 Hz, 1H), 7.00 (d, J = 10.9 Hz, 1H), 6.91 (d, J = 7.5 Hz, 1H), 6.89 (s, 1H), 6.29 (s, 1H), 5.75 (s, 1H), 4.28 (s, 2H), 3.81 (t, J = 6.3 Hz, 2H), 3.77 (s, 3H), 3.62–3.55 (m, 2H), 3.34–3.25 (m, 2H), 2.44–2.37 (m, 2H), 2.33 (t, J = 7.3 Hz, 4H), 1.72–1.64 (m, 2H), 1.57–1.49 (m, 2H). ^{13}C NMR (125 MHz, DMSO-d_6) δ(ppm): 173.58, 169.01, 168.43, 159.56, 147.51, 140.50, 137.82, 130.12, 119.28, 115.55, 112.63, 111.36, 69.09, 59.77, 57.52, 55.68, 26.82, 22.96. HRMS (*m*/*z*) calcd. For $C_{22}H_{28}N_2O_6$ [M + H]$^+$ 417.2026, found 417.2032.

3.5.6. 2-(Hydroxymethyl)-5-(4-(4-(4-methoxybenzoyl)piperazin-1-yl)butoxy)-4*H*-pyran-4-one (3f). Yellow sticky; Yield: 39.81%; 98.5% purity; IR (KBr, ν/cm^{-1}):3361, 2936, 1659, 1650, 1633, 1613, 1515, 1454, 1258, 1021, 842, 763. ^{1}H NMR (400 MHz, DMSO-d_6) δ (ppm): 8.09 (s, 1H), 7.34 (d, J = 8.2 Hz, 2H), 6.97 (d, J = 8.2 Hz, 2H), 6.29 (s, 1H), 5.70 (s, 1H), 4.29 (s, 2H), 3.87–3.80 (m, 2H), 3.78 (s, 3H), 3.51–3.44 (m, 2H), 2.54–2.46 (m, 2H), 2.43–2.21 (m, 6H), 1.74–1.63 (m, 2H), 1.59–1.47 (m, 2H). ^{13}C NMR (100 MHz, DMSO-d_6) δ (ppm): 173.57, 169.29, 168.39, 160.60, 147.53, 140.55, 129.45, 128.33, 114.09, 111.39, 69.12, 59.80, 57.55, 55.70, 53.17, 26.84, 22.97. HRMS (*m*/*z*) calcd. For $C_{22}H_{28}N_2O_6$ [M + H]$^+$ 417.2026, found 417.2024.

3.5.7. 5-(4-(4-(2-Fluorobenzoyl)piperazin-1-yl)butoxy)-2-(hydroxymethyl)-4*H*-pyran-4-one (3g). Light yellow sticky; Yield: 46.78%; 98.1% purity; IR (KBr, ν/cm^{-1}): 3271, 2940, 1645, 1613, 1454, 1295, 1150, 1132, 757. ^{1}H NMR (500 MHz, DMSO-d_6) δ (ppm): 7.97 (s, 1H), 7.41–7.32 (m, 1H), 7.26 (t, J = 6.9 Hz, 1H), 7.17 (d, J = 8.6 Hz, 1H), 7.16–7.12 (m, 1H), 6.17 (s, 1H), 5.65 (s, 1H), 4.16 (s, 2H), 3.68 (t, J = 6.3 Hz, 2H), 3.55–3.48 (m, 2H), 3.10–3.05 (m, 2H), 2.31–2.25 (m, 2H), 2.25–2.20 (m, 2H), 2.20–2.14 (m, 2H), 1.61–1.51 (m, 2H), 1.46–1.35 (m, 2H). ^{13}C NMR (ppm): (125 MHz, DMSO-d_6) δ 173.59, 168.44, 164.29, 156.98, 147.51,

140.49, 131.85, 129.25, 125.42, 116.32, 111.35, 69.08, 59.77, 57.48, 53.33, 52.75, 47.06, 26.81, 22.95. HRMS (*m*/*z*) calcd. For $C_{21}H_{25}FN_2O_5$ $[M + H]^+$ 405.1826, found 405.1825.

3.5.8. 5-(4-(4-(3-Fluorobenzoyl)piperazin-1-yl)butoxy)-2-(hydroxymethyl)-4*H*-pyran-4-one (3h). Light yellow sticky; Yield: 28.96%; 97.9% purity; IR (KBr, ν/cm^{-1}):3305, 3081, 2939, 2817, 1651, 1644, 1614, 1445, 1266, 1208, 1148, 1025, 796, 688. ^{1}H NMR (500 MHz, DMSO-d_6) δ (ppm): 7.98 (s, 1H), 7.41–7.35 (m, 1H), 7.17 (t, J = 7.6 Hz, 1H), 7.13–7.07 (m, 2H), 6.18 (s, 1H), 5.65 (s, 1H), 4.17 (s, 2H), 3.70 (t, J = 6.3 Hz, 2H), 3.53–3.45 (m, 2H), 3.22–3.13 (m, 2H), 2.34–2.26 (m, 2H), 2.25–2.16 (m, 4H), 1.61–1.52 (m, 2H), 1.46–1.37 (m, 2H). ^{13}C NMR (125 MHz, DMSO-d_6) δ (ppm): 168.44, 167.86, 163.26, 161.31, 147.51, 140.51, 131.16, 123.40, 116.73, 114.26, 111.36, 69.10, 59.77, 57.49, 26.82, 22.95. HRMS (*m*/*z*) calcd. For $C_{21}H_{25}FN_2O_5$ $[M + H]^+$ 405.1826, found 405.1828.

3.5.9. 5-(4-(4-(4-Fluorobenzoyl)piperazin-1-yl)butoxy)-2-(hydroxymethyl)-4*H*-pyran-4-one (3i). Reddish brown sticky; Yield: 32.92%; 97.2% purity; IR (KBr, ν/cm^{-1}): 3389, 2938, 2824, 1659, 1650, 1633, 1454, 1262, 1226, 1155, 1032, 850, 761. ^{1}H NMR (400 MHz, DMSO-d_6) δ (ppm): 8.09 (s, 1H), 7.48–7.42 (m, 2H), 7.30–7.23 (m, 2H), 6.29 (s, 1H), 5.77 (s, 1H), 4.28 (s, 2H), 3.81 (t, J = 6.4 Hz, 2H), 3.67–3.53 (m, 2H), 3.25–3.09 (m, 2H), 2.44–2.27 (m, 6H), 1.77–1.63 (m, 2H), 1.59–1.47 (m, 2H). ^{13}C NMR (100 MHz, DMSO-d_6) δ (ppm): 173.56, 168.44, 164.18, 161.73, 147.52, 140.56, 132.82, 130.02, 115.74, 111.38, 69.12, 59.78, 57.51, 49.06, 26.83, 22.97. HRMS (*m*/*z*) calcd. For $C_{21}H_{25}FN_2O_5$ $[M + H]^+$ 405.1826, found 405.1822.

3.5.10. 5-(4-(4-(2-Chlorobenzoyl)piperazin-1-yl)butoxy)-2-(hydroxymethyl)-4*H*-pyran-4-one (3j). Reddish brown sticky; Yield: 56.38%; 98.8% purity; IR (KBr, ν/cm^{-1}): 3563, 2943, 1667, 1612, 1506, 1434, 1295, 1211, 1149, 1032, 772, 682. ^{1}H NMR (500 MHz, DMSO-d_6) δ (ppm): 8.07 (s, 1H), 7.50 (d, J = 7.5 Hz, 1H), 7.46–7.37 (m, 2H), 7.37–7.31 (m, 1H), 6.29 (s, 1H), 5.77 (s, 1H), 4.28 (s, 2H), 3.80 (t, J = 6.5 Hz, 2H), 3.52–3.43 (m, 4H), 3.10 (t, J = 5.0 Hz, 2H), 2.45–2.38 (m, 2H), 2.33–2.29 (m, 2H), 1.72–1.63 (m, 2H), 1.58–1.47 (m, 2H). ^{13}C NMR (125 MHz, DMSO-d_6) δ (ppm): 173.61, 168.44, 165.89, 147.51, 140.45, 136.22, 129.85, 129.56, 128.34, 128.06, 111.34, 69.08, 59.78, 57.50, 53.18, 52.67, 49.06, 46.74, 26.81, 22.95. HRMS (*m*/*z*) calcd. For $C_{21}H_{25}ClN_2O_5$ $[M + H]^+$ 421.1530, found 421.1532.

3.5.11. 5-(4-(4-(3-Chlorobenzoyl)piperazin-1-yl)butoxy)-2-(hydroxymethyl)-4*H*-pyran-4-one (3k). Reddish brown sticky; Yield: 33.75%; 98.1% purity; IR (KBr, ν/cm^{-1}): 3381, 2938, 2823, 1657, 1650, 1644, 1614, 1454, 1260, 1207, 1149, 1079, 1032, 765, 742, 679. ^{1}H NMR (400 MHz, DMSO-d_6) δ (ppm): 8.06 (s, 1H), 7.51–7.39 (m, 3H), 7.31 (d, J = 7.4 Hz, 1H), 6.26 (s, 1H), 5.68 (s, 1H), 4.26 (s, 2H), 3.79 (t, J = 5.8 Hz, 2H), 3.66–3.50 (m, 2H), 3.29–3.19 (m, 2H), 2.43–2.34 (m, 2H), 2.34–2.20 (m, 4H), 1.72–1.60 (m, 2H), 1.56–1.45 (m, 2H). ^{13}C NMR (100 MHz, DMSO-d_6) δ (ppm): 168.39, 167.70, 147.52, 140.56, 138.55, 133.67, 130.93, 129.86, 127.15, 125.94, 111.39, 69.12, 59.80, 57.48, 53.25, 49.07, 26.83, 22.97. HRMS (*m*/*z*) calcd. For $C_{21}H_{25}ClN_2O_5$ $[M + H]^+$ 421.1530, found 421.1528.

3.5.12. 5-(4-(4-(4-Chlorobenzoyl)piperazin-1-yl)butoxy)-2-(hydroxymethyl)-4*H*-pyran-4-one (3l). Light yellow sticky; Yield: 23.41%; 98.2% purity; IR (KBr, ν/cm^{-1}): 3352, 2937, 1651, 1454, 1262, 1150, 1088, 1012, 840, 755. ^{1}H NMR (400 MHz, DMSO-d_6) δ (ppm): 8.06 (s, 1H), 7.47 (d, J = 8.0 Hz, 2H), 7.38 (d, J = 8.0 Hz, 2H), 6.26 (s, 1H), 5.70 (s, 1H), 4.26 (s, 2H), 3.78 (t, J = 6.4 Hz, 2H), 3.65–3.49 (m, 2H), 3.41–3.30 (m, 2H), 2.43–2.34 (m, 2H), 2.34–2.23 (m, 4H), 1.71–1.60 (m, 2H), 1.56–1.44 (m, 2H). ^{13}C NMR (100 MHz, DMSO-d_6) δ (ppm): 159.37, 148.85, 146.12, 137.32, 132.51, 130.71, 122.66, 120.90, 119.72, 118.05, 113.57, 110.96, 106.35, 74.08, 70.16, 60.49, 40.56. HRMS (*m*/*z*) calcd. For $C_{21}H_{25}ClN_2O_5$ $[M + H]^+$ 421.1530, found 421.1531.

3.5.13. 5-(4-(4-(2-Bromobenzoyl)piperazin-1-yl)butoxy)-2-(hydroxymethyl)-4*H*-pyran-4-one (3m). Light yellow sticky; Yield: 33.56%; 97.5% purity; IR (KBr, ν/cm^{-1}): 3389, 2940, 2821, 1650, 1633, 1454, 1258, 1208, 1149, 1032, 748, 665, 637. ^{1}H NMR (500 MHz, DMSO-d_6) δ (ppm): 8.08 (s, 1H), 7.66 (d, J = 7.9 Hz, 1H), 7.45 (t, J = 7.3 Hz, 1H), 7.35 (d, J = 7.5 Hz, 1H), 7.34–7.29 (m, 1H), 6.29 (s, 1H), 5.72 (s, 1H), 4.28 (s, 2H), 3.80 (t, J = 5.9 Hz, 2H), 3.67–3.60 (m, 2H), 3.12–3.06 (m, 2H), 2.47–2.39 (m, 2H), 2.38–2.25 (m, 4H), 1.77–1.62 (m, 2H), 1.58–1.46 (m, 2H). ^{13}C NMR (125 MHz, DMSO-d_6) δ (ppm): 173.58, 168.39, 166.73, 147.51, 138.40, 132.97, 131.03, 128.52, 128.32, 118.82, 111.35, 69.07, 59.80, 57.50, 53.12, 52.61, 49.07, 26.81, 22.95. HRMS (*m*/*z*) calcd. For $C_{21}H_{25}BrN_2O_5$ $[M + H]^+$ 465.1025, found 465.1027.

3.5.14. 5-(4-(4-(3-Bromobenzoyl)piperazin-1-yl)butoxy)-2-(hydroxymethyl)-4*H*-pyran-4-one (3n). Reddish brown sticky; Yield: 42.20%; 97.2% purity; IR (KBr, ν/cm^{-1}):3363, 2939, 1681, 1645, 1454, 1258, 1149, 1149, 1032, 800, 739, 671. ^{1}H NMR (500 MHz, DMSO-d_6) δ (ppm): 8.08 (s, 1H), 7.67–7.61 (m, 1H), 7.56 (d, J = 1.8 Hz, 1H), 7.42–7.36 (m, 2H), 6.29 (s, 1H), 4.29 (s, 2H), 3.81 (t, J = 6.4 Hz, 2H), 3.65–3.55 (m, 4H), 3.31–3.25 (m, 2H), 2.44–2.38 (m, 2H), 2.34–2.31 (m, 2H), 1.72–1.62 (m, 2H), 1.58–1.48 (m, 2H). ^{13}C NMR (125 MHz, DMSO-d_6) δ (ppm): 173.60, 168.42, 167.62, 147.51, 140.48, 138.70, 132.76, 131.16, 129.95, 122.17, 111.35, 69.09, 59.79, 57.48, 49.07, 26.82, 22.95. HRMS (*m*/*z*) calcd. For $C_{21}H_{25}BrN_2O_5$ $[M + H]^+$ 465.1025, found 465.1023.

3.5.15. 5-(4-(4-(4-Bromobenzoyl)piperazin-1-yl)butoxy)-2-(hydroxymethyl)-4*H*-pyran-4-one (3o). Light yellow sticky; Yield: 31.72%; 98.6% purity; IR (KBr, ν/cm^{-1}): 3332, 3085, 2942, 1650, 1614, 1454, 1258, 1150, 1066, 836, 753, 625. ^{1}H NMR (500 MHz, DMSO-d_6) δ (ppm): 8.09 (s, 1H), 7.64 (d, J = 8.2 Hz, 2H), 7.34 (d, J = 8.2 Hz, 2H), 6.29 (s, 1H), 5.74 (s, 1H), 4.28 (s, 2H), 3.81 (t, J = 6.3 Hz, 2H), 3.64–3.52 (m, 2H), 3.32–3.22 (m, 2H), 2.44–2.37 (m, 2H), 2.36–2.26 (m, 4H), 1.72–1.63 (m, 2H), 1.57–1.49 (m, 2H). ^{13}C NMR (125 MHz, DMSO-d_6) δ (ppm): 173.57, 168.42, 168.34, 147.51, 140.50, 135.53, 131.90, 129.61, 123.31, 111.36, 69.09, 59.78, 57.49, 26.82, 22.96. HRMS (*m*/*z*) calcd. For $C_{21}H_{25}BrN_2O_5$ $[M + H]^+$ 465.1025, found 465.1026.

3.5.16. 2-(Hydroxymethyl)-5-(4-(4-(2-(trifluoromethyl) benzoyl)piperazin-1-yl)butoxy)-4*H*-pyran-4-one (3p). Reddish brown sticky; Yield: 35.94%; 97.5% purity; IR (KBr, ν/cm^{-1}): 3389, 2943, 2823, 1660, 1650, 1613, 1454, 1317, 1260, 1176, 1032, 774. ^{1}H NMR (500 MHz, DMSO-d_6) δ (ppm): 7.95 (s, 1H), 7.67 (d, J = 7.9 Hz, 1H), 7.60 (d, J = 7.6 Hz, 1H), 7.51 (s, 1H), 7.31 (d, J = 7.7 Hz, 1H), 6.16 (s, 1H), 5.62 (s, 1H), 4.15 (s, 2H), 3.67 (t, J = 6.5 Hz, 2H), 3.52–3.44 (m, 2H), 3.00–2.86 (m, 2H), 2.35–2.28 (m, 1H), 2.25–2.15 (m, 4H), 2.10–2.03 (m, 1H), 1.59–1.49 (m, 2H), 1.44–1.34 (m, 2H). ^{13}C NMR (125 MHz, DMSO-d_6) δ (ppm): 173.58, 168.44, 166.45, 147.51, 140.46, 135.26, 133.34, 129.91,

127.89, 111.34, 69.07, 59.77, 57.49, 52.69, 52.55, 49.05, 47.14, 41.60, 26.79, 22.94. HRMS (*m*/*z*) calcd. For $C_{22}H_{25}F_3N_2O_5$ $[M + H]^+$ 455.1794, found 455.1796.

3.5.17. 2-(Hydroxymethyl)-5-(4-(4-(3-(trifluoromethyl) benzoyl)piperazin-1-yl)butoxy)-4*H*-pyran-4-one (3q). Light yellow sticky; Yield: 53.96%; 98.2% purity; IR (KBr, ν/cm^{-1}): 3443, 2921, 1667, 1650, 1613, 1454, 1337, 1072, 1032, 749, 702. ^{1}H NMR (400 MHz, DMSO-d_6) δ (ppm): 8.09 (s, 1H), 7.82 (d, J = 6.6 Hz, 1H), 7.76–7.62 (m, 3H), 6.29 (s, 1H), 5.73 (s, 1H), 4.28 (s, 2H), 3.81 (t, J = 6.4 Hz, 2H), 3.70–3.55 (m, 2H), 3.32–3.23 (m, 2H), 2.47–2.38 (m, 2H), 2.38–2.28 (m, 4H), 1.74–1.63 (m, 2H), 1.59–1.47 (m, 2H). ^{13}C NMR (100 MHz, DMSO-d_6) δ (ppm): 159.37, 148.85, 146.12, 137.32, 132.51, 130.71, 122.66, 120.90, 119.72, 118.05, 113.57, 110.96, 106.35, 74.08, 70.16, 60.49, 40.56. HRMS (*m*/*z*) calcd. For $C_{22}H_{25}F_3N_2O_5$ $[M + H]^+$ 455.1794, found 455.1791.

3.5.18. 2-(Hydroxymethyl)-5-(4-(4-(4-(trifluoromethyl) benzoyl)piperazin-1-yl)butoxy)-4*H*-pyran-4-one (3r). Yellow sticky; Yield: 31.08%; 98.6% purity; IR (KBr, ν/cm^{-1}): 3499, 2938, 1667, 1614, 1573, 1454, 1366, 1032, 853, 729. ^{1}H NMR (500 MHz, DMSO-d_6) δ (ppm): 8.09 (s, 1H), 7.81 (d, J = 7.9 Hz, 2H), 7.60 (d, J = 7.9 Hz, 2H), 6.29 (s, 1H), 5.78 (s, 1H), 4.28 (s, 2H), 3.81 (t, J = 6.5 Hz, 2H), 3.66–3.59 (m, 2H), 3.28–3.22 (m, 2H), 2.46–2.39 (m, 2H), 2.37–2.27 (m, 4H), 1.73–1.64 (m, 2H), 1.57–1.48 (m, 2H). ^{13}C NMR (125 MHz, DMSO-d_6) δ (ppm): 173.59, 168.46, 167.98, 147.51, 140.51, 130.19, 128.18, 125.98, 125.95, 111.35, 69.09, 59.76, 57.48, 26.82, 22.96. HRMS (*m*/*z*) calcd. For $C_{22}H_{25}F_3N_2O_5$ $[M + H]^+$ 455.1794, found 455.1792.

3.6. *In vitro* tyrosinase inhibition

The mushroom tyrosinase inhibitory activity was determined according to previous described method.[41,42] Briefly, 168 μL of phosphate buffer (0.1 M, pH 6.8), 10 μL of mushroom tyrosinase (0.5 mg mL^{-1}, Sigma Chemical, USA) and 2 μL of the inhibitor solution were placed in the wells of a 96-well micro plate. After pre-incubation for 20 min at 37 °C, 20 μL of 2.0 mg mL^{-1} *L*-DOPA (3,4-dihydroxyphenylalanine, Sigma Chemical, USA) was added and the enzyme activity was measured at 475 nm every 60 seconds for 180 seconds in a Microplate Reader (Bio-Rad Laboratories, Inc., Hercules, CA, USA). Kojic acid and phosphate buffer were respectively used as positive and negative control. The extent of inhibition by the test compounds was expressed as the percentage of concentration necessary to achieve 50% inhibition (IC_{50}). The percentage of inhibition was calculated as follows: inhibitory rate (%) = $[(A_c - A_t)/A_c] \times 100$. A_c is the absorbance of the negative control and A_t is the absorbance of the test compound. Each concentration was analyzed in three independent experiments run in triplicate. The IC_{50} values were determined by the data analysis software GraphPad Prism 8.

3.7. Tyrosinase kinetic analysis

To study the inhibition type of kojic acid–triazole derivatives, the investigation of inhibitory type of selected compound **3o** on mushroom tyrosinase was carried out according to reported protocol.[41,42] Compound **3o** was used at the concentrations of 0 μM, 2 μM and 4 μM, respectively. Substrate *L*-DOPA concentration was between 500 μM and 1000 μM in the process of all kinetic study. Pre-incubation time and measurement time were the same as described in mushroom tyrosinase inhibition assay procedure. Lineweavere–Burk plots of inverse of velocities (1/*V*) *versus* inverse of substrate concentration 1/[S] μM^{-1} was used to determine the type of enzyme inhibition.

3.8. Measurements of fluorescence spectra

To investigate the fluorescence quenching role of the inhibitor on tyrosinase, fluorescence experiments were carried out according to the reported method.[31,32] To determine the linear concentration range of the fluorescence, compound **3o** was first dissolved in DMSO. The concentration of the solution was 1.0 mM, which was then diluted with sodium phosphate buffer. The final concentration was ranged from 0 to 90 μM. A series of 2.5 mL solutions containing 0.2 mL of tyrosinase solution were added to a centrifuge tube and accurately mixed with different concentrations of **3o** solution ranging from 0 to 90 μM. Cary Eclipse G9800A fluorescence spectrophotometer (Agilent Technologies Co) was employed to detect the fluorescence intensity. The excitation wavelength was set to 280 nm, the bath was set at three temperatures (298 K, 304 K and 310 K) with a scanning wavelength range from 300 to 500 nm. The excitation and emission bandwidths were 5 nm. The final tyrosinase concentration was 0.2 mg mL^{-1}.

3.9. FT-IR spectrum measurements

A Nicolet-iS5 spectrophotometer was used to collect FT-IR spectra with germanium attenuated total reflection (ATR) based on the reported method.[43] 0.5 mg mL^{-1} tyrosinase in PBS buffer solution, pH = 6.8 PBS buffer solution and 10 μM compound **3o** in DMSO was used in the experiment. Tyrosinase solution and complex solution were smeared on KBr tablets for spectral measurement respectively. The spectra of tyrosinase and compound **3o**–tyrosinase complex were measured with the wavenumber of 4000–500 cm^{-1}, a resolution of 4 cm^{-1}, and 64 scans. The blank PBS buffer solution was measured as the baseline. The compositions of tyrosinase's secondary structures were analyzed using PeakFit software.

3.10. *In silico* docking simulation of tyrosinase with compound 3o

Molecular docking calculations were performed molecular docking calculations by using the X-ray structure of mushroom tyrosinase (PDB ID: 2Y9X) and human tyrosinase (PDB ID:5 M8M) in complex with tyrosinase inhibitor.[42] The most potent compound **3o** was prepared by conducting Prepare Ligands procedure (Discovery studio 2019) in its neutral form and preferential conformation was obtained in the CHARMm force field. Choosing one of the eight monomers from the PDB entry, and the protein structure was prepared using the Prepare Protein module in Discovery studio 2019 software, the specific steps included adding missing residues and hydrogen atoms as well as removing water molecules and spectator ions. Then their conformation optimized in the CHARMm force field. The

search grid of binding site was identified as center_*x*: −10.021, center_*y*: −28.823, and center_*z*: −43.596 with radius value of 10. Molecular modeling simulations were performed with CDOCKER protocol (Discovery studio 2019), reporting the top 10 poses for each ligand and the graph generation was done by PyMOL (Schrödinger).

3.11. Anti-browning experiment

Fuji apples were planted in Yantai of Shandong province, China, and were purchases from a Walmart supermarket in Shaoyang, Hunan province, China. The apples were from the same batch having similar shapes, maturity, and without injuries, rot, diseases or pests. Apples was cut into thin slices with the same size by using a sharp knife. Then, the fresh-cut slices were then randomly divided into different groups: the blank control group was immersed in ethanol for 10 minutes at room temperature, the treatment groups were dipped in a solution of compound **13t** under the same conditions, the positive groups were dipped in 50 μM kojic acid and 50 μM Vitamin C (V_C) under the same conditions. The test samples were air-dried naturally, immediately packaged separately in polyethylene clam-shell packs, and stored at 5 °C for the following experimental measurements.

According to the reported protocol,[41] the color of apples was tested using a CR-400 Minolta chroma meter instrument (Konica Minolta, Osaka, Japan). Three data of L^*, a^*, and b^* were recorded for each sample. The L^* values indicate lightness, the a^* values show reddish–greenish, the b^* values represent yellowish–bluish. The color measurement was carried out in triplicate by random sampling.

3.12. DPPH free radical scavenging activity assay

The anti-oxidation effect on DPPH radical was determined using a slightly modified version of a previously described DPPH radical scavenging assay.[44] The reaction mixture consisted of 100 μL DPPH (150 μM) and 20 μL test compound at different concentrations, and then the volume was adjusted to 200 μL with DMSO. The tested solution was incubated for 30 minutes at room temperature (25 °C) in a dark environment. After incubating, a UV-2600 spectrophotometer was used to measure the absorbance at 517 nm. The experiments were performed in triplicate. DMSO was used as a control, and ascorbic acid was used as an antioxidant standard for comparison. The calculation of DPPH radical scavenging activity was carried out by this formula:

DPPH radical scavenging activity (%) = (absorbance of standard − absorbance of sample)/absorbance of standard × 100

3.13. ABTS radical cation scavenging activity assay

According to the reported procedure,[45] ABTS free radical scavenging activity was assayed. The test solution was prepared by mixing 2.45 mM potassium persulfate and 7 mM ABTS in an 8 : 12 (volume ratio). The reaction solution was kept for 12 to 18 hours at room temperature in the dark. Before the ABTS radical scavenging test, the reaction mixture was diluted with DMSO to the absorbance of 0.7 ± 0.02 at 734 nm. 1 mL diluted ABTS test solution was added to 10 μl DMSO or test sample solution. After mixing, the mixture was kept for 2 to 6 minutes in the dark at room temperature, and the absorbance at 734 nm was tested. This measurement was performed in triplicate. DMSO was used as a blank control. Ascorbic acid was used as antioxidant standard to compare the ABTS scavenging activity. The ABTS scavenging activity was calculated by following formula:

ABTS scavenging activity (%) = (absorbance of standard − absorbance of sample)/absorbance of standard × 100

3.14. MTT assay for cell viability

The cytotoxic activity of compound **3o** against the HUVEC cell line (purchased from Shanghai iCell Bioscience Inc) using 3-(4,5-dimethylthiazol-2-yl)-2,5- diphenyltetrazolium bromide (MTT) assay. HUVEC cell line was cultured in Dulbecco's modified Eagle's medium (DMEM, Gibco-BRL, Gaithersburg, MD, USA), which was supplemented with 10% fetal bovine serum (FBS) and 1% penicillin/streptomycin. Cells were cultured in a standard humidified incubator at 37 °C with a 5% CO_2 atmosphere. Cells were plated in 96-well microtiter plates at a density of 5×10^3 per well and incubated in a humidified atmosphere with 5% CO_2 at 37 °C for 24 h. Compound **3o** was added onto triplicate wells with different concentrations and 0.1% DMSO used for the control. After they had been incubated for 48 h, 10 μL of CCK8 (Cell Counting Kit-8) solution was added to each well, and the plate was incubated for an additional 1 h. The absorbance (OD) was read on a microplate reader at 450 nm.

$$\text{Cell viability (\%)} = [(A_{\text{sample}} - A_{\text{blank}})/(A_{\text{control}} - A_{\text{blank}})] \times (100)$$

A_{sample} denotes the OD_{450} absorbance of test compound and A_{blank} is the OD_{450} absorbance for the blank. A_{control} represents the OD_{450} absorbance of control.[32,38]

4. Conclusions

In this study, we designed and synthesized eighteen kojic acid–piperazine derivatives, with their structures fully characterized by NMR, IR, and HRMS. The yields of target compounds ranged from 23.41% to 53.96%. All compounds were evaluated for tyrosinase inhibitory activity, with compound **3o** demonstrating the most potent inhibition ($IC_{50} = 0.21 \pm 0.01$ μM). Preliminary structure–activity relationship analysis revealed: Substituents on the benzene ring showed limited improvement in inhibitory activity; For electron-donating groups, *ortho*-substitution exhibited optimal activity while *meta*-substitution showed the weakest effects; For electron-withdrawing groups, *para*-substituted derivatives displayed superior activity; Smaller halogen atomic radii correlated with reduced potency; Stronger electron-donating capacity potentially diminished inhibitory

effects. Mechanistic studies on the lead compound **3o** confirmed its competitive inhibition mode through kinetic analysis. Fluorescence quenching and FT-IR spectroscopy demonstrated interactions between compound **3o** and C=O and N–H bonds of tyrosinase. Molecular docking revealed that: the kojic acid moiety coordinates with the active-site copper ions and interacts with key amino acid residues. The piperazine ring forms π–π interactions with surrounding residues. Additionally, compound **3o** exhibited notable anti-browning effects and low cytotoxicity. In addition, while some compounds showed moderate DPPH radical scavenging activity, most displayed negligible ABTS scavenging capacity. However, no significant correlation was observed between tyrosinase inhibitory activity and antioxidant activity. These findings provide valuable insights for developing novel tyrosinase inhibitors with improved efficacy.

Author contributions

Meiqun Ye performed research and drafted the manuscript. Meiqun Ye, Xiqian Xie and Yinxing Chen synthesized all target compounds. Hui Jiang and Meiqun Ye tested the *in vitro* bioactivity. Meiqun Ye, Man Ren performed the computational work and interpreted the data. Jinbing Liu conceived and supervised the overall project and revised the manuscript. All authors have read and approved the final text and consent to its publication.

Conflicts of interest

The authors declare that they have no known competing financial interests or personal relationships that could have appeared to influence the study reported in this paper.

Data availability

The supporting data has been provided as part of the supplementary information (SI). Supplementary information: ^{1}H and ^{13}C NMR spectra for the synthesized compounds. See DOI: https://doi.org/10.1039/d5ra08323k.

Acknowledgements

The authors are grateful for the funding support provided by National Undergraduate Training Program on Innovation and Entrepreneurship (S202310547022), Hunan Provincial Natural Science Foundation of China (2025JJ70200) and Aid Program for Science and Technology Innovative Research Team in Higher Educational Institutions of Hunan Province (Xiangjiaotong [2023] No. 233).

References

1 S. Zolghadri, A. Bahrami, M. T. Hassan-Khan, *et al*, Comprehensive review on tyrosinase inhibitors, *J. Enzym. Inhib. Med. Chem.*, 2019, **34**, 279–309.
2 A. Mermer and S. Demirci, Recent advances in triazoles as tyrosinase inhibitors, *Eur. J. Med. Chem.*, 2023, **259**, e115655.
3 J. Choi, Y.-M. Lee and J.-G. Jee, Thiopurine drugs repositioned as tyrosinase inhibitors, *Int. J. Mol. Sci.*, 2018, **19**, 77–92.
4 Q. Yu, L. Fan and Z. Duan, Five individual polyphenols as tyrosinase inhibitors: inhibitory activity, synergistic effect, action mechanism, and molecular docking, *Food Chem.*, 2019, **297**, e124910.
5 L. Ielo, B. Deri, M. P. Germanò, *et al*, Exploiting the 1-(4-fluorobenzyl)piperazine fragment for the development of novel tyrosinase inhibitors as anti-melanogenic agents: Design, synthesis, structural insights and biological profile, *Eur. J. Med. Chem.*, 2019, **178**, 380–389.
6 Y. Nazir, A. Saeed and M. Rafiq, Hydroxyl substituted benzoic acid/cinnamic acid derivatives tyrosinase inhibitory kinetics, anti-melanogenic activity and molecular docking studies, *Bioorg. Med. Chem. Lett.*, 2020, **30**, e126722.
7 J. Li, L. Feng, L. Liu, *et al*, Recent advances in the design and discovery of synthetic tyrosinase inhibitors, *Eur. J. Med. Chem.*, 2021, **224**, e113744.
8 N. H. Nasab, H. Raza, Y. S. Eom, *et al*, Synthesis and discovery of potential tyrosinase inhibitor of new coumarin-based thiophenyl-pyrazolylthiazole nuclei: *In vitro* evaluation, cytotoxicity, kinetic, and computational studies, *Chem. Biol. Drug Des.*, 2023, **101**, 1262–1272.
9 L. Patrycja, G. Waldemar, H. Katarzyna, *et al*, Tripeptides conjugated with thiosemicarbazones: new inhibitors of tyrosinase for cosmeceutical use, *J. Enzym. Inhib. Med. Chem.*, 2023, **38**, e2193676.
10 A. Ortiz-Urquiza and N. O. Keyhani, Action on the surface: entomopathogenic fungi *versus* the insect cuticle, *Insects*, 2013, **4**, 357–374.
11 N. M. Khoa, N. V. Phong, S. Y. Yang, *et al*, Spectroscopic analysis, kinetic mechanism, computational docking, and molecular dynamics of active metabolites from the aerial parts of *Astragalus membranaceus* Bunge as tyrosinase inhibitors, *Bioorg. Chem.*, 2023, **134**, e106464.
12 D. W. Wen, C. C. Li, H. Di, *et al*, A universal HPLC method for the determination of phenolic acids in compound herbal medicines, *J. Agric. Food Chem.*, 2005, **53**, 6624–6629.
13 O. A. R. Rodríguez, N. E. M. Vergara, A. R. Organillo, *et al*, Synthesis, crystal structure, antioxidant activity and dft study of 2- aryl-2,3-dihydro-4H-[1,3]thiazino [3,2-a] benzimidazol-4-one, *J. Mol. Struct.*, 2020, **1199**, e127036.
14 V. Kumar, K. Vaid, K. M. Kim, *et al*, Advancements in metal organic framework-based materials for the detection of antioxidants in food and biological fluids, *Trend. Anal. Chem.*, 2024, **171**, e117522.
15 G.-L. Chen, M.-X. Fan, M.-Q. Guo, *et al*, Antioxidant and anti-inflammatory properties of flavonoids from lotus plumule, *Food Chem.*, 2019, **277**, 706–712.
16 L. D. Luca, M. P. Germanò, A. Fais, *et al*, Discovery of a new potent inhibitor of mushroom tyrosinase (Agaricus bisporus) containing 4-(4-hydroxyphenyl)piperazin- 1-yl moiety, *Bioorg. Med. Chem.*, 2020, **28**, e115497.

17 N. Mohammadsadeghi, A. Mahdavi, F. Saadati, *et al*, *In silico* and *in vitro* studies of novel derivatives of tyrosol and raspberry ketone as the mushroom tyrosinase inhibitors, *Food Chem.*, 2023, **424**, e136413.
18 A. M. Muddathir, K. Yamauchi, I. Batubara, *et al*, Anti-tyrosinase, total phenolic content and antioxidant activity of selected Sudanese medicinal plants, *J. S. Afr. Bot.*, 2017, **109**, 9–15.
19 S. Ranjbar, S. Razmara, M. Khoshneviszadeh, *et al*, 6-(Hydroxymethyl) -8-oxo-4,8-dihydropyrano[3,2-b]pyrans as new tyrosinase inhibitors and antioxidant agents, *ChemistrySelect*, 2023, **8**, e202302990.
20 J. C. Zilles, F. L. Santos, R. V. Contri, *et al*, Biological activities and safety data of kojic acid and its derivatives: A review, *Exp. Dermatol.*, 2022, **31**, 1500–1521.
21 G. C. Wang, M. He, Y. Huang and Z. Y. Peng, Synthesis and biological evaluation of new kojic acid-1,3,4-oxadiazole hybrids as tyrosinase inhibitors and their application in the anti-browning of fresh-cut mushrooms, *Food Chem.*, 2023, **409**, e135275.
22 M. He, M. Fan, W. Liu, *et al*, Design, synthesis, molecular modeling, and biological evaluation of novel kojic acid derivatives containing bioactive heterocycle moiety as inhibitors of tyrosinase and antibrowning agents, *Food Chem.*, 2021, **362**, e130241.
23 M. D. Santi, M. A. Peralta, M. Puiatti, *et al*, Melanogenic inhibitory effects of Triangularin in B16F0 melanoma cells, *in vitro* and molecular docking studies, *Bioorg. Med. Chem.*, 2019, **27**, 3722–3728.
24 S. Radhakrishnan, R. Shimmon, C. Conn, *et al*, Design, synthesis and biological evaluation of hydroxy substituted amino chalcone compounds for antityrosinase activity in B16 cells, *Bioorg. Chem.*, 2015, **62**, 117–123.
25 S. Lee, S. Ullah, C. Park, *et al*, Inhibitory effects of N-(acryloyl) benzamide derivatives on tyrosinase and melanogenesis, *Bioorg. Med. Chem.*, 2019, **27**, 3929–3937.
26 S. M. Hashemi and S. Emami, Kojic acid-derived tyrosinase inhibitors: synthesis and bioactivity, *Pharm. Biomed. Res.*, 2015, **1**, 1–17.
27 S. Emami, R. Ahmadi, H. Ahadi, *et al*, Diverse therapeutic potential of 3-hydroxy-4-pyranones and related compounds as kojic acid analogs, *Med. Chem. Res.*, 2022, **31**, 1842–1861.
28 H. S. Rho, H. S. Baek, S. M. Ahn, *et al*, Synthesis and biological evaluation of kojyl thioether derivatives as tyrosinase inhibitors, *B. Korean Chem. Soc.*, 2010, **31**, 2375–2378.
29 W. Xie, J. Zhang, X. Ma, *et al*, Synthesis and biological evaluation of kojic acid derivatives containing 1,2,4-triazole as potent tyrosinase inhibitors, *Chem. Biol. Drug Des.*, 2015, **86**, 1087–1092.
30 Z. Peng, G. Wang, J. J. Wang, *et al*, Anti-browning and antibacterial dual functions of novel hydroxypyranone-thiosemicarbazone derivatives as shrimp preservative agents: Synthesis, bio-evaluation, mechanism, and application, *Food Chem.*, 2023, **419**, e136106.
31 Y. Lou, Z. Peng, J. Tang, *et al*, Study on the synthesis and biological activity of kojic acid triazol thiosemicarbazide Schiff base derivatives, *J. Enzym. Inhib. Med. Chem.*, 2025, **40**, e2475071.
32 D. Liu, J. Tang, T. Sheng, *et al*, Design, synthesis and biological evaluation of novel kojic acid triazole hybrids as tyrosinase inhibitors and antibrown- ing agents, *Sci. Rep.*, 2025, **15**, e15005.
33 G. Karakaya, A. Ture and A. Ercan, Synthesis, computational molecular docking analysis and effectiveness on tyrosinase inhibition of kojic acid derivatives, *Bioorg. Chem.*, 2019, **88**, e102950.
34 D. Cigdem, O. T. Fulya, B. O. Serap, *et al*, Newly synthesized piperazine derivatives as tyrosinase inhibitors: *in vitro* and *in silico* studies, *J. Iran. Chem. Soc.*, 2022, **19**, 2739–2748.
35 J. A. Wiles, B. J. Bradbury and M. J. Pucci, New quinolone antibiotics: a survey of the literature from 2005 to 2010, *Expert Opin. Ther. Pat.*, 2010, **20**, 1295–1319.
36 M. Baumann and I. R. Baxendale, An overview of the synthetic routes to the best selling drugs containing 6-membered heterocycles, *Beilstein J. Org. Chem.*, 2013, **9**, 2265–2319.
37 M. T. Varela, E. V. C. Levatti, A. G. Tempone, *et al*, Investigation of structure–activity relationships for benzoyl and cinnamoyl piperazine/piperidine amides as tyrosinase inhibitors, *ACS Omega*, 2023, **8**, 44265–44275.
38 F. Ricci, K. Schira, L. D. Luca, *et al*, Computational methods to analyze and predict the binding mode of inhibitors targeting both human and mushroom tyrosinase, *Eur. J. Med. Chem.*, 2023, **260**, e115771.
39 R. Romagnoli, P. Oliva, F. Prencipe, *et al*, Cinnamic acid derivatives linked to arylpiperazines as novel potent inhibitors of tyrosinase activity and melanin synthesis, *Eur. J. Med. Chem.*, 2022, **231**, e114147.
40 H. J. Tang, P. Song, J. Li, *et al*, Effect of Salvia miltiorrhiza on acetylcholinesterase: enzyme kinetics and interaction mechanism merging with molecular docking analysis, *Int. J. Biol. Macromol.*, 2019, **135**, 303–313.
41 W. Zhou, F. Wu and J. Liu, Biological evaluation and synthesis of thiazole Sch-iff base derivatives, *Heterocycles*, 2021, **102**, 1337–1353.
42 J. Tang, J. Liu and F. Wu, Molecular docking studies and biological evaluation of 1,3,4-thiadiazole derivatives bearing Schiff base moieties as tyrosinase inhi- bitors, *Bioorg. Chem.*, 2016, **69**, 29–36.
43 J. Chen, Z. Zhang, H. Li, *et al*, Exploring the effect of a series of flavonoids on tyrosinase using integrated enzyme kinetics, multispectroscopic, and molecular modelling analyses, *Int. J. Biol. Macromol.*, 2023, **252**, e126451.
44 Z. Peng, G. Wang, Q.-H. Zeng, *et al*, Synthesis, antioxidant and anti-tyrosinase activity of 1,2,4-triazole hydrazones as antibrowning agents, *Food Chem.*, 2021, **341**, e128265.
45 Y.-M. Chen, C. Li, W.-J. Zhang, *et al*, Kinetic and computational molecular docking simulation study of novel kojic acid derivatives as antityrosinase and antioxidant agents, *J. Enzym. Inhib. Med. Chem.*, 2019, **34**, 990–998.